# AC Loss Calculation for Litz Wire Windings in Electrical Machines

Wenjun Zhu, *Graduate Student Member, IEEE*, Yangyu Sun, Xiao Chen, *Senior Member, IEEE*, Jiabin Wang, *Senior Member, IEEE*, G. W. Jewell, Ellis Chong, and Andreas Reeh

Abstract—High-frequency operation of electrical machines leads to excessive AC losses in the windings due to skin and proximity effects. To mitigate these losses, multistrand windings or Litz wire windings can be employed. This paper explores the applicability of the direct finite element (FE) method and two computationally efficient approaches—the homogenization technique and the FE-based dB/dt technique—for predicting Litz wire AC losses in electrical machines. Experimental validation is conducted using a motorette model with different configurations. Based on the dB/dt technique, a fast sweep method is proposed for AC loss calculation across various Litz wire specifications. This method efficiently scales with variations in working points, enabling the optimal design of Litz wire over a working cycle to minimize winding losses in a computationally efficient manner.

Index Terms— AC loss, Litz wire, high-speed machines.

#### I. INTRODUCTION

High-speed electrical machines are emerging techniques in the more electric aircraft and electrical vehicles (EVs) and by offering superior power density, efficiency, and lightweight designs. In EV traction machines, hairpin windings are increasingly used due to their high slot fill factor, improved thermal performance, and manufacturing repeatability. However, with maximum speeds reaching ~25,000rpm and even exceeding ~30,000rpm [1], AC losses in electrical machines become significant due to increased skin and proximity effects. In aerospace applications, most electrical machines operate at high frequencies (>1 kHz) due to either high pole pair number or high rotational speed, making AC losses a critical concern [2]. The high AC losses caused by eddy currents induced in the winding conductors can lead to high winding temperature and premature insulation failure. Litz wires which have multistrand, enamelled and weaved wires, can be employed to reduce AC losses at high frequencies.

In literature, various types of modelling approaches have been proposed to predict AC loss in Litz wire with round conductors. One-dimensional (1D) Dowell's Equation was proposed in [3] to predict AC winding resistance in a transformer originally. An equivalent square conductor sheet is used to approximate round conductors. J. Ferreira [4] and M. Albach [5] used Bessel function to account for curvature and thus directly calculated the eddy currents for round conductors when they are exposed in air with a two-dimensional (2D) analytical solution. Based on the above methods, many other papers further improved the analytical methods by accounting for slot leakage, fringing effect, 3D effect etc. [6-10].

Numerical analysis with direct finite element (FE) method using solid conductors can provide direct solutions for AC loss calculation. However, for Litz wire applications, the computational demand is remarkably high considering each strand needs a reasonable discretization. This is particularly challenging if the magnetic field is 3-dimentional (3D), as in the end-winding regions of an electrical machine.

Homogenization technique has been developed in [11-14] to model Litz wire as homogeneous region using frequency dependent resistivity and complex permeability. Then, the Litz wire AC loss can be calculated using an AC solver. Time domain homogenization technique were developed in [15, 16]. The eddy current reaction field effect on AC loss calculation can be accounted with homogenization techniques, while no stranded discretization is needed. This method requires the winding to have regular patterns in both directions perpendicular to the current direction to satisfy their boundary conditions.

FE based analytical approaches have been developed in [17-19] to extract flux densities from FE solution before using analytical equations to predict the AC loss. Eddy current reaction field effect on AC loss calculation is neglected in this approach.

Apart from the modelling techniques, the design guides of Litz wire applications have not been well reported. C. R. Sullivan [20] proposed a power law to model insulation thickness in the winding region, which, when combined with eddy-current loss models, yields an analytic solution for the optimal number of strands for transformer applications but not for electrical machines. Litz wire manufacturers will also give some guidelines about how to choose the appropriate strand

This work was supported in part by Rolls-Royce plc. (Corresponding author: Xiao Chen).

Wenjun Zhu is with the University of Sheffield, Sheffield, S10 4DE, UK (e-mail: wzhu24@ sheffield.ac.uk).

Yangyu Sun is with the University of Sheffield, Sheffield, S10 4DE, UK (e-mail: ysun78@sheffield.ac.uk).

Xiao Chen is with the University of Sheffield, Sheffield, S10 4DE, UK (e-mail: xiao.chen@sheffield.ac.uk).

Jiabin Wang is with the University of Sheffield, Sheffield, S10 4DE, UK (e-mail: j.b.wang@sheffield.ac.uk).

Geraint W. Jewell is with the University of Sheffield, Sheffield, S10 4DE, UK (e-mail: g.jewell@sheffield.ac.uk).

Ellis Chong is with Rolls-Royce Electrical, Derby, DE24 8BJ, UK (e-mail: ellis.chong@rolls-royce-electrical.com).

Andreas Reeh is with Rolls-Royce Electrical, Munich, Otto-Hahn Ring 6, 81739 Germany (e-mail: andreas.reeh@rolls-royce-electrical.com).

diameter of a Litz wire for a given operating frequency range. This is mainly with concern that the strand diameter should be less than the skin depth to mitigate the skin effects loss.

This paper first validates the homogenization technique, and the FE based dB/dt technique through the comparison with direct FE calculation in simulation. Apart from the active windings, the AC losses in the end windings are investigated with 3D FE model of a representative motorette. Experiment validations are performed with air core and iron core setups. For the iron core experimental setup, a novel differential method is proposed to eliminate the effects of iron loss.

Furthermore, based on the dB/dt technique, computationally efficient method is proposed for selection of Litz wire windings in the design phase to sweep 1) all the available Litz wire specifications and 2) different working points. The novelty of this method lies in identifying the decoupling between geometric parameters (strand diameter and slot fill factor) and the magnetic field (dB/dt). Consequently, the AC loss in Litz wire windings can be expressed as a function of strand diameter, while incorporating geometric constraints and ensuring scalability with flux density and frequency. This finding enables easy scalability to different working points, allowing for quick optimization of Litz wire design over a single working cycle to minimize total winding losses.

# II. SIMULATION COMPARISON OF DIFFERENT COMPUTATION METHODS

# A. Direct FE computation

Modelling electrical machines equipped with Litz wire, which usually consists of several tens or hundreds or even thousands of strands, can be difficult and time-consuming in finite element analysis (FEA) software even for the model with periodicity because each strand needs to be discretized finely to capture the skin and proximity effect. In addition, the competition of geometrical model and the building of associated electrical circuit are also time-consuming. Given the restriction on CPU speed and available RAM on a typical PC nowadays (e.g. Intel(R) Core™ i9-10900X CPU @ 3.70GHz and 32GB RAM), direct FE transient computation involving rotor movement should be performed only when it is very necessary.

Alternatively, a simplified model without movement of rotor using a steady state AC solver is sufficient to perform the benchmark comparison of various modelling approaches. A 96 slots permanent magnet (PM) machine with stack length of 300mm was studied. As shown in Fig. 1, a motorette model (with dimensions marked in mm) is modelled in Altair Flux with 10 turns of Litz wire winding. Each bundle consists of 115 strands with a diameter of 0.4mm following a hexagonal pattern distribution as shown in Fig. 2(a). The mesh density is illustrated in Fig. 2(b), and each strand conductor has multiple layers of mesh elements to capture the skin effect. Another possible rectangular pattern of strands is shown in Fig. 2(c) which may have a lower fill factor at the bundle level.

A perfect Litz wire refers to that the strands in a Litz wire are enameled and weaved, and they successively pass through all points of the bundle cross-section in order to ensure that the current will share equally among the separate strands. To simulate this, all strands are assumed to be connected in series and subject to a single current source. Due to the twisted nature of the strands in Litz wires, the actual length of each strand is longer than the depth of the domain in a 2D FEA model. This effect can be evaluated using the twist factor, which will be discussed in Section III indicated by DC resistance measurements.

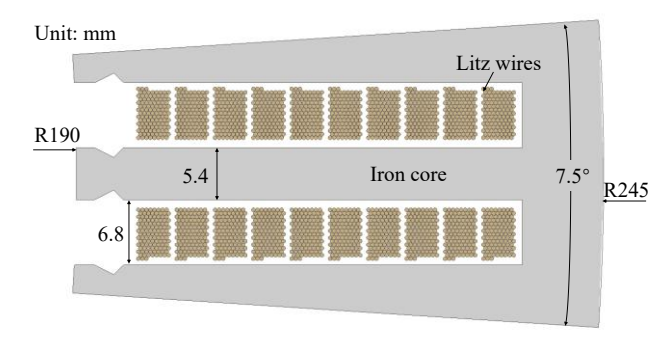
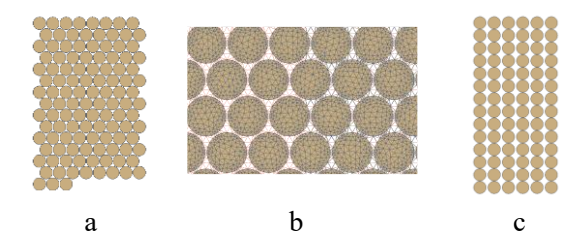


Fig. 1. Motorette model with 10 turns Litz wire winding.



**Fig. 2.** A bundle of Litz wire. (a) hexagonal pattern distribution of strands; (b) zoom in view of mesh elements of strands; (c) rectangular pattern distribution of strands.

# B. Homogenization technique

The homogenization technique models the Litz wire area as a uniform region with frequency-dependent resistivity and complex permeability, eliminating the need for strand-level discretization [14]. This method leverages the periodic arrangement of strands to efficiently represent eddy current effects using equivalent material properties.

The process consists of pre-processing and FEA of the homogenization model. In pre-processing, equivalent resistivity is derived from a single-strand model, while complex permeability is determined using a quarter-strand model under an external magnetic field. Both models run in 2D FEA with an electromagnetic AC solver. In FEA, the homogenized properties are assigned to the coil material to compute proximity losses, while the skin effect resistance is incorporated into the resistance matrix to account for total AC losses [11] [12].

Altair Flux offers a built-in homogenization feature for modelling multi-strand conductors or Litz wires. As illustrated in Fig. 3 for the motorette model, the windings can be represented as a block region, eliminating the need for detailed strand-level modelling.

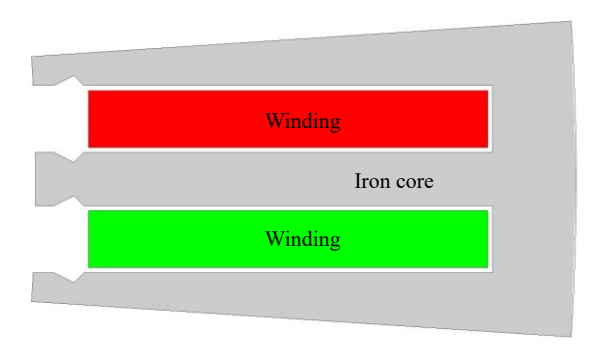


Fig. 3. Motorette model with winding blocks without strands modelled.

# C. FE based dB/dt technique

For a given strand diameter d, the base frequency  $f_b$  is defined when the skin depth is equal to the strand diameter [21]:

$$f_b = \frac{1}{\pi \mu \sigma d^2} \tag{1}$$

where  $\mu$  is the material permeability and  $\sigma$  is the material conductivity.

When the frequency is below the base frequency, the reaction field of eddy current can be neglected. Based on this assumption, the FE based dB/dt technique can be derived with analytical formulas. The formulas are summarized as follows.

Strand level skin effect loss refers to the eddy current loss caused by the source current in a strand. The strand-level skin effect gravimetric loss density of a round conductor caused by arbitrary current can be expressed as [19]:

$$p_{skin}(t) = \frac{d^4(\pi\mu)^2 \sigma}{1536} \frac{1}{2\pi^2} \left(\frac{dJ_z}{dt}\right)^2 \tag{2}$$

where d is the strand diameter and  $J_z(t)$  is the time-variable current density.

Assuming sinusoidal AC current, the time-averaged strand level skin loss density can be rewritten as:

$$\bar{p}_{skin} = \frac{d^4(\pi\mu)^2 \sigma}{1536} J_{mz}^2 f^2$$
 (3)

where f is the frequency and  $J_{mz}$  is the amplitude of the sinusoidal current density.

Strand level proximity loss is caused by the eddy currents due to the magnetic field produced by the current in other strands and other external magnetic fields, e.g., the rotor permeant magnets.

Strand level proximity loss density,  $p_{prox}$ , of a round conductor can be expressed as:

$$p_{prox}(t) = \frac{\pi^2 d^2 \sigma}{8} \frac{1}{2\pi^2} \frac{d\vec{B}_n}{dt} \cdot \frac{d\vec{B}_n}{dt} + \frac{\pi^2 d^2 \sigma}{16} \frac{1}{2\pi^2} \frac{d\vec{B}_l}{dt} \cdot \frac{d\vec{B}_l}{dt}$$
(4)

where  $\overrightarrow{B_n}$  is the flux density normal to the strand, and  $\overrightarrow{B_l}$  is the flux density tangential to the strand, as shown in Fig. 4.

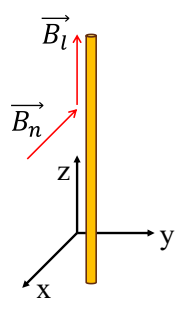


Fig. 4. Components of flux density and their directions with respect to a strand.

In Cartesian coordinates,  $\vec{B} = [B_x, B_y, B_z]$  and the proximity loss density can be expressed as:

$$p_{prox}(t) = \frac{d^2\sigma}{16} \frac{d\overrightarrow{B_x}}{dt} \cdot \frac{d\overrightarrow{B_x}}{dt} + \frac{d^2\sigma}{16} \frac{d\overrightarrow{B_y}}{dt} \cdot \frac{d\overrightarrow{B_y}}{dt} + \frac{d^2\sigma}{32} \frac{d\overrightarrow{B_z}}{dt} \cdot \frac{d\overrightarrow{B_z}}{dt}$$
 (5)

In sinusoidal magnetic field, the time-averaged strand level proximity loss density can be rewritten into:

$$\bar{p}_{prox} = \frac{\pi^2 d^2 \sigma}{8} B_{mx}^2 f^2 + \frac{\pi^2 d^2 \sigma}{8} B_{my}^2 f^2 + \frac{\pi^2 d^2 \sigma}{16} B_{mz}^2 f^2$$
 (6)

where  $B_{mx}$ ,  $B_{my}$  and  $B_{mz}$  are the magnitudes of flux density components in the x, y, and z directions, respectively. The total loss will be volumetric integration of the winding region and time average (integration) over a fundamental electrical period.

As can be seen, both the skin and proximity loss densities are proportional to  $\sigma$  and  $f^2$ . However, the skin effect loss density is also proportional to  $d^4$  and  $\mu^2$  while the proximity loss density is proportional to  $d^2$ . For most Litz wire strand, d is typical below 1mm and  $\mu \approx \mu_0 = 4\pi \times 10^{-7} \text{H/m}$ . Consequently, with representative current density and slot leakage flux density in an electrical machine, the skin loss component is much lower than the proximity loss component when the frequency is below the base frequency of the Litz wire.

With the above analytical equations, the AC loss calculation can be performed by extracting flux density from FE calculations and the FE model does not need to discretize each strand shown in Fig. 1. Instead, it only requires modelling winding blocks (Fig. 3) with uniform current density and zero conductivity. This technique has indeed been employed in Ansys Maxwell for evaluation of AC losses in stranded conductors and Litz wires [19]. When using the built-in feature for AC loss calculation in Ansys Maxwell, the Litz wires are assumed to be evenly distributed within the slot. The  $\frac{d\vec{B}}{dt} \cdot \frac{d\vec{B}}{dt}$ values are then computed and summed across all mesh elements in the slot region. However, this differs from the actual magnetic flux density inside the strands, as the precise position of each strand remains unknown. Furthermore, this is a postprocess after FEA, which means the strand diameter and number of strands per bundle are not involved in the magnetic field calculation.

#### D. Motorette results comparison

The calculations are performed with 2D steady state AC solver at various frequencies. To ensure consistency, the model geometry, boundary condition and all relevant parameters are set to be the same as those of the detailed stranded motorette

model. The core is made of silicon steel M270-35A with a stack length of 300mm.

Direct FE computation was performed using a detailed stranded model with a second-order mesh, totaling 487,482 mesh elements, while the blocked model used only 6,402 mesh elements. Fig. 5 shows the current density distribution in the stranded model at 1000Hz and 57.5A rms per bundle (equivalent to 4 A/mm² as air cooling condition). From the visualization, it is evident that the current density is unevenly distributed across the winding. Higher concentrations appear near the edges of the conductors in the bundles nearest to the slot opening. This observation aligns with the flux density distribution in the winding region of the blocked winding model, as shown in Fig. 6. The strands located nearer to the slot opening experience higher flux density.

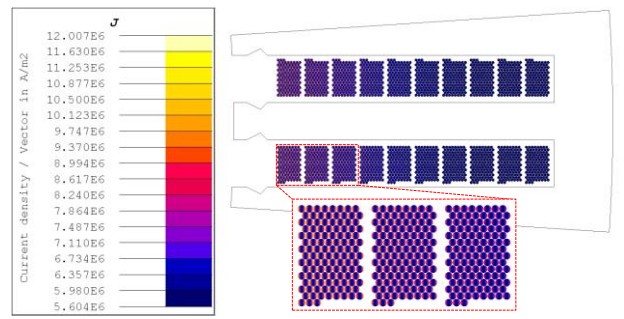


Fig. 5. Current density distribution at 1000Hz with 57.5A rms using direct FEA.

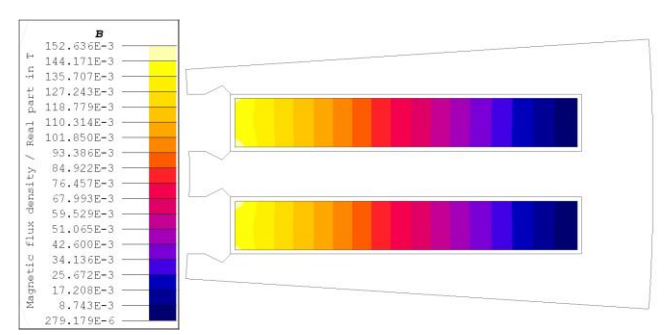


Fig. 6. Flux density distribution at 1000Hz with 57.5A rms using blocked winding model.

Fig. 7 compares the total winding AC resistance (normalized to the DC resistance of 2D model) calculated by Altair Flux using the homogenization technique, Ansys Maxwell using the dB/dt technique, and the direct FE method at 57.5Arms per bundle. The AC resistance predicted by the three methods shows good agreement with each other below the base frequency  $f_b = 27.3 \text{kHz}$ . However, the dB/dt technique tends to overestimate the AC loss above the base frequency, due to the fact that the eddy current reaction field is not accounted in the dB/dt technique as shown in Table I. It is also important to appreciate that the AC loss by the homogenization approach is still quite close to that by the direct FE model at  $2f_b$  and  $3f_b$ . Hence the homogenisation is more suitable for AC loss estimation at higher frequency than  $f_b$ . This is advantageous when the AC loss associated with PWM operation is to be evaluated.

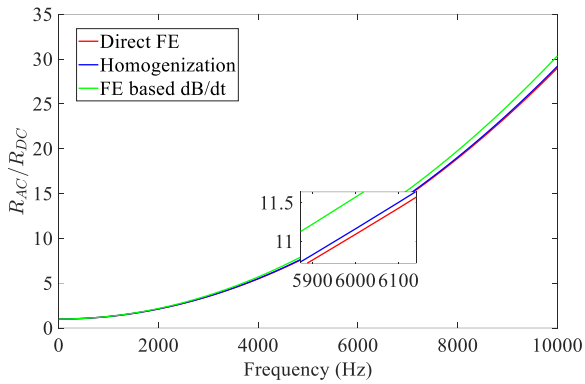


Fig. 7. Comparison of total winding resistance for the motorette model.

With 32GB RAM and Intel(R) Core(TM) i9-10900X 3.70 GHz CPU, the computation time of 50 frequency points are presented in Table II, which shows the advantages of the computationally efficient techniques (homogenization and dB/dt).

TABLE I. Comparison of AC Resistance at  $f_b$ ,  $2f_b$  and  $3f_b$ 

Frequency		Direct FE	Homogenization	FE based dB/dt
£	$R_{AC}/R_{DC}$	208.1	209.6	219.9
Jb	%	-	+0.7%	+5.7%
2.6	$R_{AC}/R_{DC}$	806.1	813.1	876.7
$2f_b$	%	-	+0.9%	+8.8%
$3f_b$	$R_{AC}/R_{DC}$	1730.8	1749.0	1971.3
	%	-	+1.1%	+13.9%

TABLE II. COMPUTATION TIME COMPARISON

Software	Altair Flux	Altair Flux	Ansys Maxwell
Method	Direct FE	Homogenization	FE based dB/dt
Computation time	~4 hours 34 min	~22 min	~4 min

It follows that the two computationally efficient techniques yield quite accurate AC loss predictions when the frequency is below the base frequency of the Litz wire, while their model complexity and computation time are significantly reduced. These computationally efficient techniques have been integrated in the commercial electromagnetic tools and hence the AC loss associated with machine windings employing Litz wire can be evaluated conveniently and seamlessly in an electromagnetic design process.

# E. AC Losses in End Windings

To accurately predict the AC loss in end-windings, 3D FE analysis is needed. However, direct FE modelling of full axial length with 10 bundles at strand level is not realistic due to the computation resource limit and hence not considered for this study. 3D models with FE based dB/dt technique representing the motorette sample have been built in Ansys Maxwell as shown in Fig. 8(a). Full length 3D model which accounts for end-winding region including a straight axial coil extension. The results can be used as baseline for comparison with 2D models. And the end-winding loss can be estimated by subtracting the loss in the 2D model from those predicted by the

3D model.

It should be noted that since the proximity loss is proportional to  $B^2$  and the flux density in the end-winding region is expected to be much smaller than that of the active parts as shown in Fig. 8(b). This phenomenon would infer a much lower AC loss in the end windings than in the active region.

The total winding AC resistances predicted by the 3D model and the 2D model are presented in Fig. 9 along with the difference (refer to the right axis) which represents the losses in the end windings. All the resistance values are normalized to the DC resistance of 2D model. The result implies that the AC loss in the end-winding is negligible in the motorette which employs a concentrated winding configuration. In general, if the end-winding length is relatively short as those typically seen in concentrated windings, neglecting AC loss in the end windings would not lead to a significant copper loss estimation error. On the other hand, in machines employing distributed winding, the AC loss needs to be assessed using one of the computationally efficient techniques with a 3D model. Alternatively, the end-winding loss may be assessed by a 2D model exposed in air with an equivalent field using one of the techniques. Such a model is of course neglecting the curvature effect and mutual flux from the other phases.

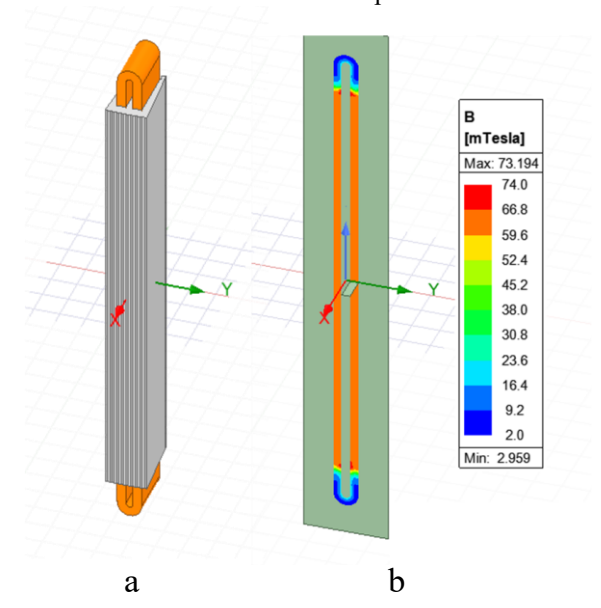


**Fig. 8.** 3D FE analysis of the motorette model in Ansys Maxwell (3D). (a) Geometrical model. (b) Flux density map in the coil region.

To assess the viability of the homogenization technique in a 3D context, a 3D motorette model was constructed using Altair Flux. Employing identical settings as in the FE based dB/dt counterpart on geometry, material properties, and excitation currents, the total winding AC resistance were compared in Fig. 10. At low frequencies, the AC resistance predicted by homogenization technique using Altair Flux 3D closely aligns with that of the dB/dt technique using Ansys Maxwell 3D. However, at high frequencies, a slight deviation occurs. This discrepancy is attributed to neglecting the eddy current reaction field effect in the dB/dt technique, while it is considered in the

homogenization technique. This trend is the same as the observed behavior in the AC loss comparison of these two techniques in 2D.

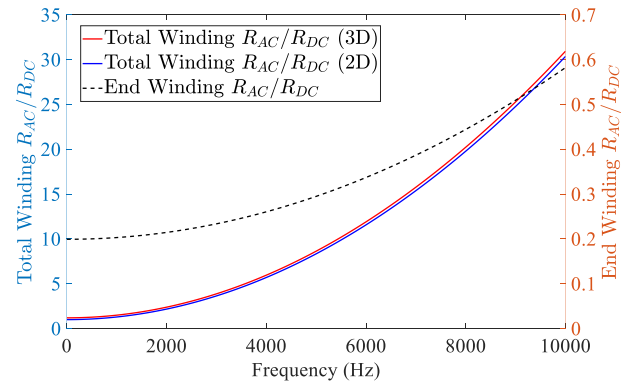


Fig. 9. End winding resistance calculated by FE based dB/dt technique.

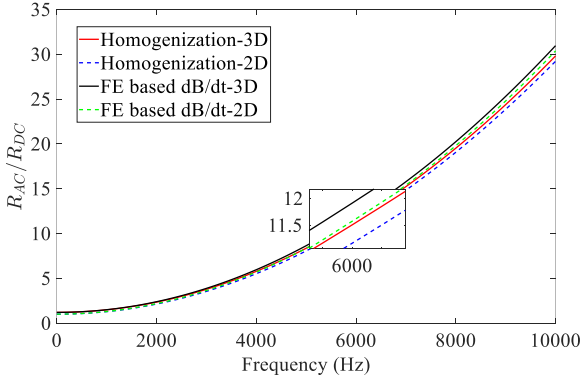


Fig. 10. Comparison of total winding AC resistance for the motorette model.

Since the 2D model does not account for the resistance of the end-winding region, the DC resistance of the end-winding was added to the AC resistance obtained from the 2D FEA models. This combined value was then compared to the results from the 3D models, as shown in Table III. A maximum difference of only 1.3% was observed at 10 kHz, indicating that the AC losses in the end-winding region are very small. Table IV compares the computation time for 50 frequency points between the 2D and 3D models. Given the minor discrepancy in AC resistance and the substantially higher computational cost of the 3D model, 3D FEA should only be used when strictly necessary for accuracy.

TABLE III. AC RESISTANCE COMPARISON OF 3D AND 2D MODELS

Method	Homogenization		FE based dB/dt			
Frequency	$2D^*$	3D	2D/3D	$2D^*$	3D	2D/3D
2kHz	16.66 mΩ	16.77 mΩ	99.3%	16.99 mΩ	17.10 mΩ	99.4%
4kHz	40.91 mΩ	41.37 mΩ	98.9%	42.22 mΩ	42.66 mΩ	99.0%
6kHz	81.32 mΩ	82.35 mΩ	98.7%	84.26 mΩ	85.25 mΩ	98.8%
8kHz	137.85 mΩ	139.70 mΩ	98.7%	143.13 mΩ	144.88 mΩ	98.8%
10kHz	210.48 mΩ	213.36 mΩ	98.7%	218.81 mΩ	221.55 mΩ	98.8%

\*AC resistance calculated from 2D FEA model + DC resistance of the end-winding region

TABLE IV. COMPUTATION TIME COMPARISON OF 3D AND 2D MODELS FOR 50 FREQUENCY POINTS

Method	Model	Computation time	
II	2D	~22 min	
Homogenization	3D	~4 hours 13 min	

FE based dB/dt	2D	~4 min
	3D	~3 hours 03min

#### III. EXPERIMENTAL VALIDATION

This section delves into an experimental investigation aimed at understanding the characteristics and performance of Litz wire. The examination comprises a series of tests and analyses designed to assess key parameters such as DC resistance, which provides insights into the twisted nature of Litz wire. Additionally, AC resistance measurements are conducted in air to eliminate the influence of iron loss, followed by AC resistance measurements with an iron core to simulate magnetic field conditions similar to those found in machine slots.

#### A. DC resistance

The DC resistance is measured with impedance analyzer Hioki IM3570 and gives the result of  $9.44 m\Omega$ . With the overall length of the Litz wire of 7.08 m, the calculated DC resistance is  $8.45 m\Omega$ . The ratio of the measured DC resistance and the calculated resistance is 1.12 and it mainly represents the twisted nature of the Litz wire. The DC resistance results are summarized in Table V.

TABLE V. DC RESISTANCE RESULTS

Measurement	Calculation	Twist factor K <sub>t</sub>
9.44 mΩ	$8.45~\mathrm{m}\Omega$	1.12

# B. Motorette test in air

To avoid the interference of iron losses, the test was first carried out with Litz wires using an air representing core. A wooden frame was manufactured to constrain the Litz wires in the position, as depicted in Fig. 11. Comparison of AC resistance results of Litz wires in the air core is shown in Fig. 12. The AC resistance was calculated using both Ansys Maxwell (FE-based dB/dt method) and Altair Flux (homogenization technique), with results subsequently scaled and adjusted for the twist factor.

It can be seen that in the medium frequency range, the measured resistance is slightly higher than the calculated results of both methods. This could be explained by the imperfect Litz wire in practice, which leads to uneven share of flux between strands and further leads to additional bundle level skin effect loss and proximity effect loss. While in higher frequency range, the calculation results with FE-based dB/dt method tend to overestimate the losses due to the neglection of eddy current reaction field.

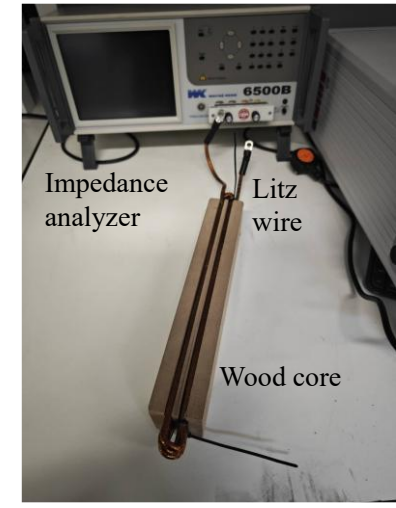


Fig. 11. Litz wire test with air (wood) core.

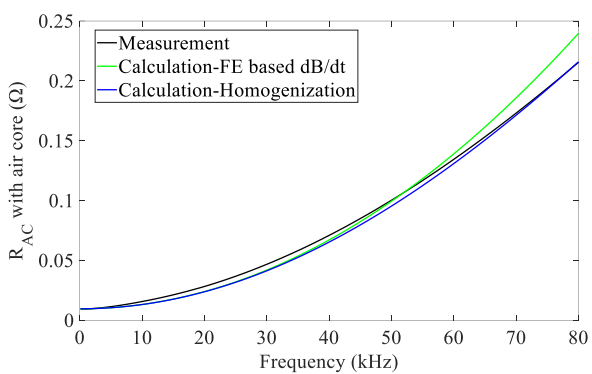


Fig. 12. Comparison of AC resistance results of Litz wires with air core.

#### C. Motorette test with iron core

However, the air core scenario cannot fully represent the electromagnetic condition of the electrical machine. Since flux density exposed to windings in machine slots is much greater than that in the air, AC loss measurement with a motorette sample is more representative to the physical condition in a machine. Hence the Litz wire with iron core of the material M250-35A, which is a typical material of laminated silicon steel used for electrical machines, was studied, as depicted in Fig. 13. In such a test sample, a higher  $R_{AC}/R_{DC}$  ratio is expected as the flux density in the slot region is higher than the one in air core. However, in this case, the measured resistance is contributed by both copper loss and iron loss. While accurately predicting iron loss in electrical machines remains a challenging task, the experimental measurement and calibration of iron loss must be a prerequisite procedure for this method for good accuracy.

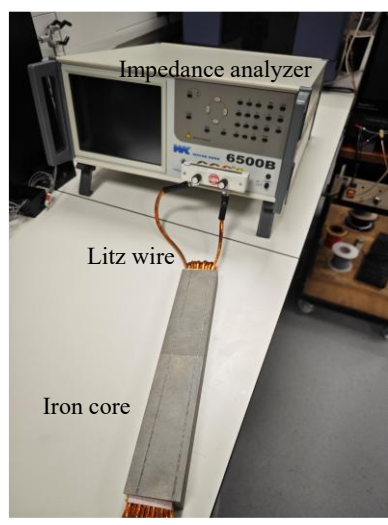


Fig. 13. Litz wire test in iron core.

To eliminate the influence of iron loss on AC loss measurements, two sets of Litz wire coils are employed, as shown in Fig. 14. In CASE1, Coil-1, consisting of 5 bundles, is placed in the slot bottom and excited. In CASE2, Coil-2, also with 5 turns (bundles), is positioned on top of Coil-1, but only Coil-1 is excited while Coil-2 remains open-circuit. At frequencies below the base frequency, the eddy current reaction field is negligible. Therefore, the presence of the open-circuit Coil-2 will not alter the magnetic field in the core when Coil-1 is excited, but proximity loss will occur in Coil-2. Consequently, the iron losses in CASE1 and CASE2 are very similar when the currents in Coil-1 are equal. The measured loss difference between CASE2 and CASE1 represents the proximity loss in Coil-2 in CASE2.

The test is conducted using the constant current mode of the impedance analyzer, Wayne Kerr 6500B which has a bandwidth of 5MHz and basic accuracy on impedance of ±0.05%. In this mode, the impedance analyzer applies a 20mArms current to excite Coil-1, ensuring uniform iron loss in both CASE1 and CASE2. The measured AC resistance of CASE1 and CASE2 is depicted in Fig. 15, with the difference also displayed on the same figure using the right axis. Subsequently, the difference is compared with the calculated AC resistance of proximity losses in Coil-2 obtained from the FE-based dB/dt technique and the homogenization method up to 10kHz, as shown in Fig. 16. The simulation results from both methods consistently underestimate the measured AC losses, primarily attributable to the imperfect Litz wire in practice.

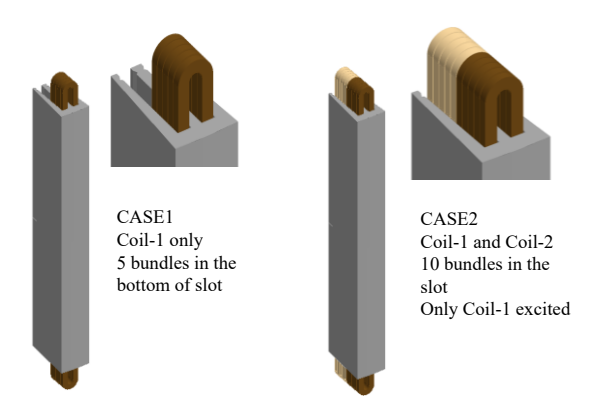


Fig. 14. Motorette test with 2 coils.

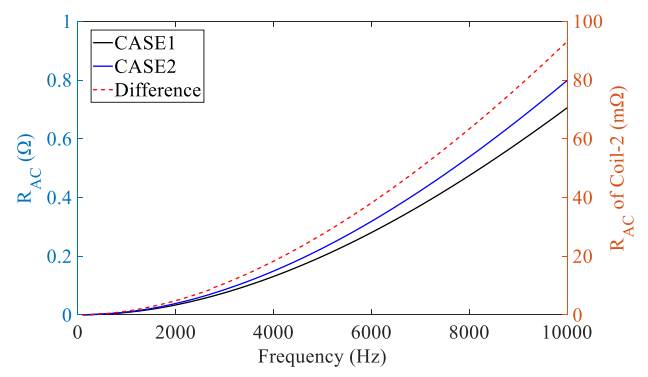


Fig. 15. Measurement results of AC resistance of CASE1 and CASE2.

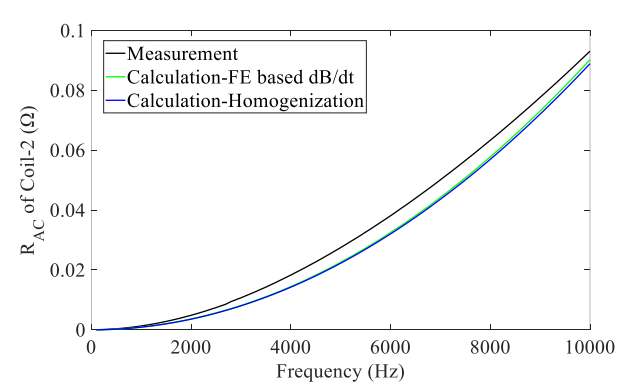


Fig. 16. Comparison of AC resistance results of proximity loss in Coil-2.

#### D. Error analysis

The implications of imperfect Litz wire arise when the strands, although enameled and weaved in a perfect Litz wire, fail to ensure equal current distribution among the separate strands.

For practical imperfect Litz wire, the internal field due to source current may cause uneven current distribution in strands within a bundle when they are connected at terminals. This leads to additional bundle level skin losses.

External fields may cause uneven current distribution in strands within a bundle when they are connected at terminals. This leads to additional bundle level proximity losses as well.

Bundle level skin effect loss due to non-perfect Litz wire is subject to the Litz wire type and manufacture and is much greater than bundle level proximity effect loss [22]. According

to the experiments reported in [22] the bundle level proximity effect loss is very small, <2%, when the wire length is greater than 3 times of the bundle pitch. This condition is typically met in an electrical machine winding.

Measurement errors occur because the pre-defined accuracy of impedance analyzer is normally based on the measured impedance Z. However, this accuracy can be much comprised in this application which has a low R/Z ratio at high frequencies. Moreover, the low  $R_{AC}/R_{DC}$  ratio is also a challenge in obtaining an accurate  $R_{AC}$  measurement. To improve the accuracy of the measured R, a capacitor bank connected in-series to compensate the reactance and thus reduce the R/Z ratio could help.

However, the two coils method which uses a motorette sample with two Litz wire coils has good potential in significantly reducing the measurement error by taking multiple measurements and average, because the AC loss in this method is taken by subtracting one loss from another and good measurement accuracy does not depend on the instrument accuracy, but its repeatability (if there are no systematic errors but only random errors left). The latter can be enhanced by multiple measurements and averaging. In this manner, biased drifting and random noise with a zero average can both be eliminated in the measurement. Therefore, the motorette with two Litz wire coils set up is recommended for experimental validation of AC loss modelling.

# IV. RAPID SCALABILITY

# A. Decoupling of strand diameter and magnetic field

As presented in [19], Ansys Maxwell computes Litz wire AC losses through post-processing. The process involves first calculating the magnetic field distribution via finite element analysis, then extracting the field values from each mesh element to feed into analytical equations for AC loss estimation. However, this approach requires re-running the FEA for every parameter variation, such as strand diameter, number of strands per bundle, excitation current, or frequency, which could be computationally expensive.

In contrast, the proposed rapid scaling method eliminates the need for repeated FEA simulations by decoupling the strand diameter from the magnetic field calculation. This significantly improves computational efficiency while maintaining accuracy.

Considering the winding skin effect loss is negligible compared to the winding proximity loss in most electrical machines, the AC loss with FE-based dB/dt technique can be represented by the spatial integral of the product of the time average of the proximity loss density in (4) and the elemental volume, as shown in (7).

$$\bar{p}_{AC} = \iint_{S} k_{F} l \int \frac{d^{2}\sigma}{16} \frac{1}{T} \left( \frac{d\vec{B}}{dt} \cdot \frac{d\vec{B}}{dt} \right) dt ds$$

$$= \frac{d^{2}\sigma}{16} k_{F} l \iint_{S} \frac{1}{T} \int \left( \frac{d\vec{B}}{dt} \cdot \frac{d\vec{B}}{dt} \right) dt ds \qquad (7)$$

$$= f(d) C_{FF}$$

where  $k_F$  is the copper fill factor and l is the axial length.

 $f(d) = \frac{d^2\sigma}{16} k_F l$  is a function of strand diameter d,  $C_{FE}$  is the time average of  $\frac{d\vec{B}}{dt} \cdot \frac{d\vec{B}}{dt}$  over the fundamental period T and then integrated on the slot area.

In FEA calculations, the slot area is discretized into many elements, so that  $C_{FE}$  can be rewritten as [19]:

$$C_{FE} = \sum_{all-elements} \left\{ \left[ \frac{1}{T} \int \left( \frac{d\vec{B}}{dt} \cdot \frac{d\vec{B}}{dt} \right) dt \right] S_{element} \right\}$$
 where  $S_{element}$  is the area of each element. (8)

Hence the AC loss is decoupled with f(d) and  $C_{FE}$ . f(d) is a function of strand diameter and fill factor.  $C_{FE}$  is subject to magnetic flux density variation rate and frequency. Note that  $C_{FE}$  is a constant at a given operating point. This means that once  $C_{FE}$  is known with one FEA solution, then the AC loss is just an analytical function of strand diameter since f(d) is independent from  $C_{FE}$ . This allows users to perform a quick sweep of all the available strand diameters either in AWG table or other customized wire specifications to understand how the strand diameter affects the Litz wire AC loss.

Given that the AC loss is proportional to  $f^2B^2$  as discussed in Section II, it is also not difficult to scale the AC loss to other working points with different frequencies and loads assuming the influence of the iron core magnetic saturation is negligible, which implies the flux density in slot is approximately proportional to current.

Taking the 48-slots 8-poles Toyota Prius IV machine (Fig. 17) as an example [23, 24], the key parameters are listed in Table VI. This machine was originally designed with hairpin windings. For demonstration purposes, the following sections will show the proposed decoupled scale method by assuming the hairpin windings are replaced with Litz wires.

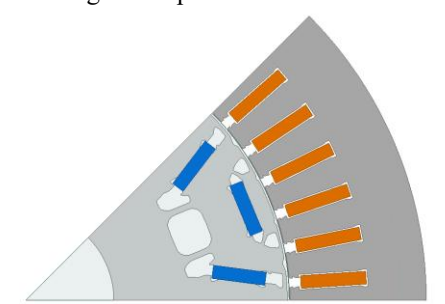


Fig. 17. The 48 slots 8 poles machine.

TABLE VI. KEY PARAMETERS OF THE PRIUS IV MACHINE

Parameters	Values	Unit
Peak power	53	kW
Peak torque	163	Nm
Max speed	17,000	rpm
DC link voltage	600	V
Stack length	59.5	mm
Air gap length	0.7	mm
Sator outer diameter	215	mm
Rotor outer diameter	140.3	mm

# B. Sweep the strand diameter

For a given working point with a certain frequency and current, the selection of Litz wire process in this study will sweep the strand diameter and output an AC loss curve as a function of the strand diameter to allow users to decide which strand diameter to choose based on their own cost function and their desirable AC to DC loss ratio.

Assume electromagnetic design of the machine has been completed, the Litz wire selection process can be undertaken for a rectangle slot shown in Fig. 18 with the following steps:

Step 1: Calculate  $C_{FE}$  at the given operating condition with one FEA solution.

Step 2: Based on the geometry information, calculate the geometrical area allocated to one bundle  $A_B$ .

Step 3: By assuming 60% of the net bundle fill factor with respect to  $A_B$  (excluding the bundle insulation), calculate the total copper area. Note that users can change this 60% fill factor to other suitable values. If assuming the insulation thickness is 0, the theoretical upper limits of fill factor are 78.5% for the rectangular pattern and 90.7% for the hexagonal pattern in geometry.

Step 4: Sweep along the available wire table with the strand diameter and find the number of strands n in one bundle (round n to an integer).

Step 5: Calculate the actual copper fill factor, DC loss, and AC loss based on n.

Step 6: Get average area occupied by one conductor  $S = A_B/n$ . For rectangle pattern shown in Fig. 19 (a) and hexagon pattern shown in Fig. 19 (b), calculate the distance between neighboring conductors x respectively. A larger x/D means it is easier to manufacture.

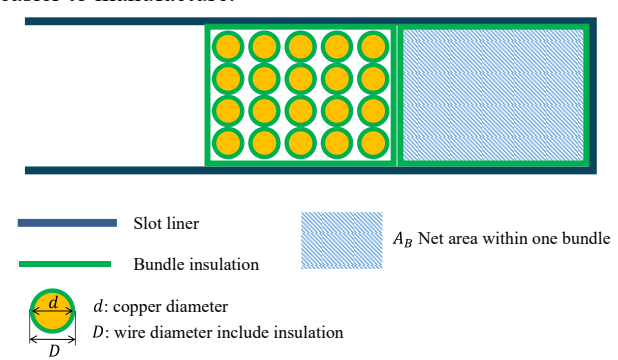


Fig. 18. Slot geometry and wire diameters.

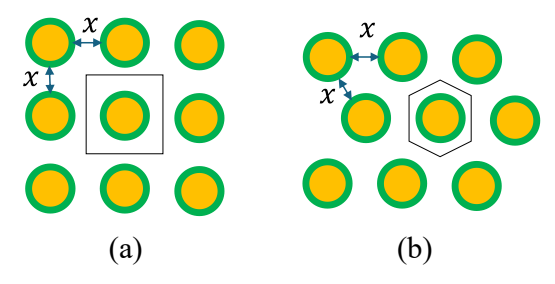


Fig. 19. Distribution patterns of conductors; (a) rectangle pattern; (b) hexagon pattern.

At 17,000rpm and 25kW operation (corresponding to 45A RMS current per bundle), the DC loss, AC loss, and total copper loss can be calculated using the proposed fast sweep method. The DC loss of the end-winding has been included based on an end-winding mean length. The slot liner thickness used in this example is assumed to be 0.5mm. The resultant DC loss, AC

loss, and total copper loss variations with respect to the strand diameter are shown in Fig. 20. With the decrease of the strand diameter, the AC loss reduces as expected while the DC loss is nearly constant. This is because the Litz wire bundle fill factor is treated as an input constant and the strand insulation thickness has not reached the condition that inter-strand gap, x, becomes zero when  $d \ge 0.1$ mm. Hence the effective copper area is constant. The fluctuation in the DC loss curve in Fig. 20 is caused by the discontinuous strand diameters in AWG table and hence a small variation of actual bundle fill factor with respect to the number of strands at a given strand diameter.

Fig. 21 shows the AC to DC loss ratio which can be used as one criterion to select the Litz wire diameter. By way of example, if the user's desirable AC to DC loss ratio is <4%, a 0.30mm strand diameter Litz wire can be chosen.

If the cost of Litz wire as a function of strand diameter is known, a weighted objective in terms of cost and AC loss can be established to select the optimal strand diameter. Further, the variation of bundle copper fill factor with strand diameter, if such information is available, can also be included in the design process. This will, indeed, be reflected in the strand separation distance, x.

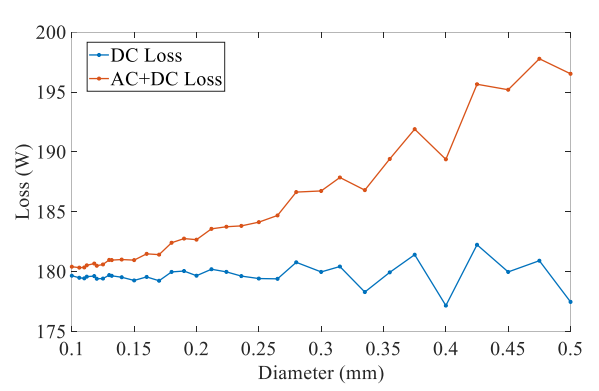


Fig. 20. Losses with respect to wire diameters.

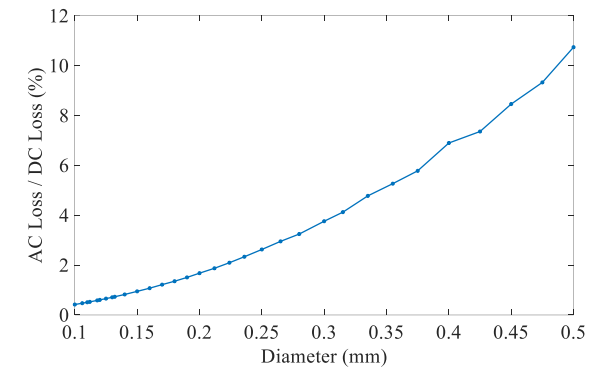


Fig. 21. AC/DC loss ratio with respect to wire diameters.

Fig. 22 shows the x/D ratio using rectangular and hexagon patterns shown in Fig. 18. It can be observed that the hexagon pattern presents a higher x/D ratio than the rectangular pattern, due to the fact that the hexagon pattern exhibits a better utilization rate of the space between strands.

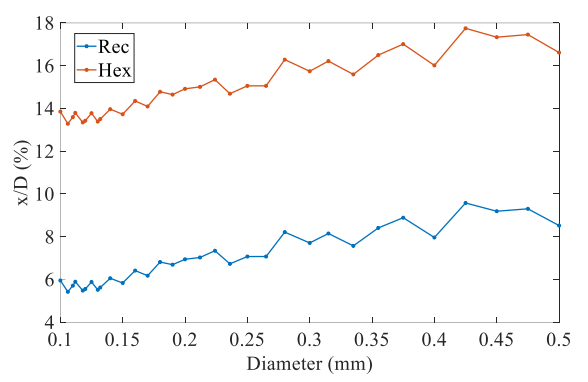


Fig. 22. Variations of x/D ratio for rectangular and hexagonal patterns with respect to strand diameters.

# C. Scale with working points

With sinusoidal current excitation, Equation (8) can be expressed as

$$C_{FE} = \sum_{all-elements} 2\pi^2 B_m^2 f^2 S_{element}$$
 where  $B_m$  is the magnitude of flux density. (9)

If the iron core is not saturated, the flux density in slot is approximately proportional to current, and hence the AC loss can be scaled to other working point with frequency or current.

Fig. 23 compares the AC losses from the proposed rapid scaling method in Section IV.A with those from Ansys Maxwell using the FE-based dB/dt method at different speeds/frequencies. The proposed rapid scaling method requires only one FEA solution, which is the AC loss at 17,000 rpm as shown in Fig. 23, and then scales this result with  $f^2$  to other working points, e.g., 4,250 rpm, 8,500 rpm, and 12,750 rpm. A good match is observed between the proposed rapid scaling method and the results from Ansys Maxwell using the FE-based dB/dt method, which involves recalculating the magnetic field at each frequency, demonstrating its scalability with frequency.

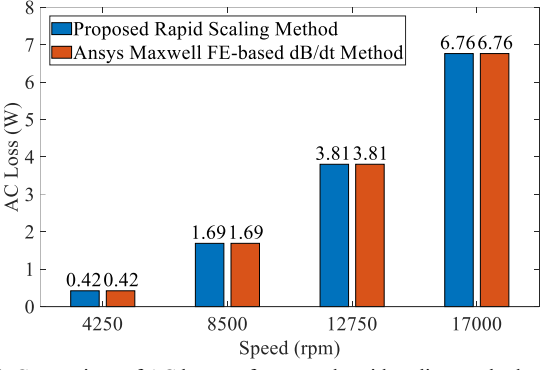


**Fig. 23.** Comparison of AC losses of proposed rapid scaling method and Ansys FE-based dB/dt method at different speeds.

Similarly, Fig. 24 compares the AC losses at different current conditions. For the proposed rapid scaling method, calculations are made based on the AC loss at 45A as the baseline and then scaled down to 22.5A and scaled up to 67.5A and 90A using  $I^2$  ratio. In contrast, the results from Ansys Maxwell's built-in feature are obtained by recalculating the magnetic field through

FEA at each current level. The close agreement between these results in Fig. 24 validates the scalability with current if the iron core is not saturated.

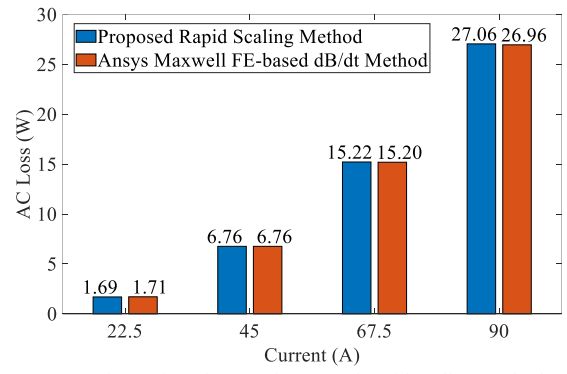


Fig. 24. Comparison of AC losses of proposed rapid scaling method and Ansys FE-based dB/dt method at different currents.

The accuracy of the proposed rapid scaling method depends on two key factors related to dB/dt:

#### 1) Frequency

The method remains accurate below the base frequency  $f_b$ , where the skin depth exceeds the strand diameter. This condition is typically met in electrical machines using Litz wire. For example,  $f_b$ =27.3 kHz for a strand diameter of 0.4 mm. In an 8-pole machine operating at 17,000 rpm, the electrical frequency is only 1,133 Hz, which is well within the valid range.

#### 2) Flux density

The rapid scaling method assumes linear magnetic behaviour, meaning flux density scales proportionally with current (i.e., negligible saturation effects). Whereas the relative permeabilities of the soft magnetic materials in the stator and rotor cores at saturation conditions are still higher than that of the winding region, the magnetic saturation at high load conditions does lead to errors in the rapid scaling method, which will be quantified in this section.

With maximum torque per ampere (MTPA) and field weakening control strategies, the *d*- and *q*-axis currents are determined for given torque and speed demands. Then, the AC losses over the machine torque-speed plane, predicted by Ansys FE based dB/dt method, are plotted in Fig. 25. Note that the maximum AC loss in Fig. 25 is lower than that in Fig. 24, because the maximum current magnitude at maximum speed in Fig. 25 is lower than that in Fig. 24. The relatively small machine-level AC losses shown in this section is because Litz wire is used in this machine to reduce AC losses.

Subsequently, using the 15,000 rpm, 20 Nm operating point as the reference for the fast scaling method, Fig. 26 demonstrates the region that the AC loss error (magnitude) between the two methods remains within a 10% bound. The red dot is the reference operating point taken for the rapid scaling method. It can be observed that the rapid scaling method can predict AC losses well at high-speed or low-torque region, while its error can exceed 10% at high torque region, primarily due to the magnetic saturation effect. The error in the low-speed and low-torque region also exceeds 10%, and this is mainly due to the fact that the AC losses in this region are very small. For

the applications in which the load torque changes frequently, multiple reference points at various representative operating regions can be used to account for the nonlinearity incurred by magnetic saturation while still saving computation time compared to using FE based dB/dt techniques at all the working points.

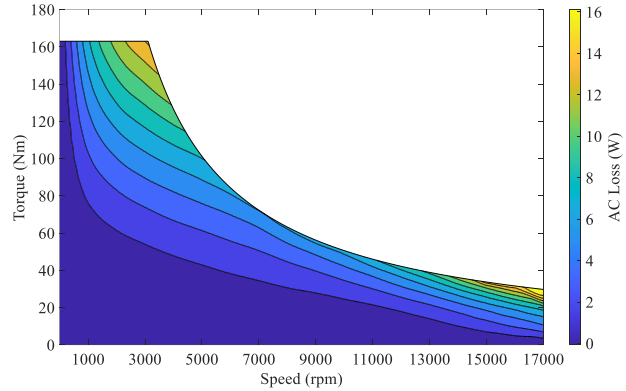
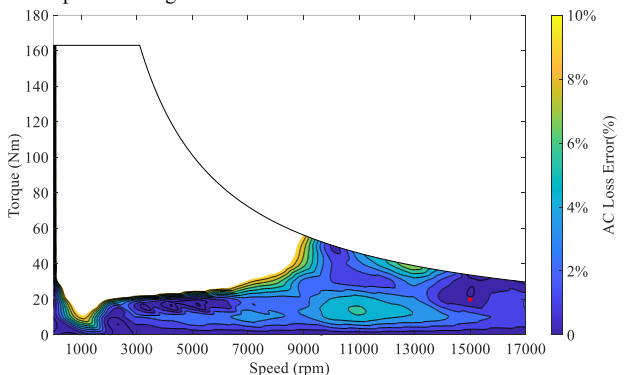


Fig. 25. AC losses prediction with Ansys FE-based dB/dt method in the machine operation range.



**Fig. 26.** Comparison of AC losses of proposed rapid scaling method and Ansys FE-based dB/dt method in the machine operation range.

#### V. CONCLUSION

In this paper, various Litz wire AC loss prediction techniques are assessed and their merits and applicability in machine winding AC loss predictions are discussed. Direct AC loss computations by 2D FE analysis are performed to understand their computational challenges with today's computing resources, and the results are also used as the reference for evaluation of two computationally efficient AC loss prediction techniques: the homogenization technique and the FE based dB/dt technique. It has been shown that when the frequency is below the base frequency at which the skin depth is equal to the strand diameter of a Litz wire, the AC losses predicted by all three techniques agree well. At higher frequencies (beyond base frequency), the homogenization technique exhibits better accuracy than the FE based dB/dt technique, considering the former accounts for eddy current reaction effects.

Furthermore, experimental tests were carried out with different setups to validate the calculation methods. A motorette model with 2 coils setup was proposed to evaluate the proximity loss. Because this method eliminates the influence of the iron loss and good measurement accuracy in this method does not

depend on the instrument accuracy but its repeatability, the latter can be enhanced by multiple measurements and averaging. It is recommended for further measurements of AC winding losses.

Using the FE based dB/dt technique, a fast analytical method has been developed to predict AC losses for different Litz wire specifications at various working points (frequency and current) for electrical machines. This method requires only one solution of the FE model if saturation effects are insignificant. Multiple reference points at various saturation levels can be considered in order to reduce the errors incurred by magnetic saturation while saving computation time. Furthermore, additional economic or manufacturing considerations can be incorporated into this method, making it a useful tool for the design of Litz wire windings.

#### REFERENCES

- [1] A. Arzillo *et al.*, "Challenges and Future opportunities of Hairpin Technologies," *2020 IEEE 29th International Symposium on Industrial Electronics (ISIE)*, Delft, Netherlands, 2020, pp. 277-282.
- [2] A. Al-Qarni, A. El-Refaie, and F. Wu, "Impact of Machine Parameters on The Design of High Specific Power Permanent Magnet Machines for Aerospace Applications," in 2021 IEEE International Electric Machines & Drives Conference (IEMDC), Hartford, CT, USA, 17-20 May 2021 2021: IEEE, pp. 1-8.
- [3] P. L. Dowell, "Effects of eddy currents in transformer windings," Proceedings of the Institution of Electrical Engineers, vol. 113, no. 8, 1966
- [4] J. A. Ferreira, "Improved analytical modeling of conductive losses in magnetic components," *IEEE Transactions on Power Electronics*, vol. 9, no. 1, pp. 127-131, 1994.
- [5] M. Albach, "Two-dimensional calculation of winding losses in transformers," in 2000 IEEE 31st Annual Power Electronics Specialists Conference, Galway, Ireland, 2000, vol. 3: IEEE, pp. 1639-1644.
- [6] N. Xi and C. R. Sullivan, "An improved calculation of proximity-effect loss in high-frequency windings of round conductors," in *IEEE 34th Annual Conference on Power Electronics Specialist*, Acapulco, Mexico, 2003, vol. 2: IEEE, pp. 853-860.
- [7] C. R. Sullivan, "Computationally efficient winding loss calculation with multiple windings, arbitrary waveforms, and two-dimensional or threedimensional field geometry," *IEEE Transactions on Power Electronics*, vol. 16, no. 1, pp. 142-150, 2001.
- [8] F. Tourkhani and P. Viarouge, "Accurate analytical model of winding losses in round Litz wire windings," *IEEE Transactions on Magnetics*, vol. 37, no. 1, pp. 538-543, 2001.
- [9] D. Winterborne, S. Jordan, L. Sjoberg, and G. Atkinson, "Estimation of AC copper loss in electrical machine windings with consideration of end effects," Gothenburg, Sweden, 2020 2020: IEEE, pp. 847-853.
- [10] A. Bardalai, X. Zhang, T. Zou, D. Gerada, J. Li, and C. Gerada, "Comparative Analysis of AC losses with round magnet wire and Litz wire winding of a High – Speed PM Machine," in 2019 22nd International Conference on Electrical Machines and Systems (ICEMS), Harbin, China, 2019 2019: IEEE, pp. 1-5.
- [11] J. Gyselinck and P. Dular, "Frequency-domain homogenization of bundles of wires in 2-D magnetodynamic FE calculations," *IEEE Transactions on Magnetics*, vol. 41, no. 5, pp. 1416-1419, 2005.
- [12] A. D. Podoltsev, K. G. N. B. Abeywickrama, Y. V. Serdyuk, and S. M. Gubanski, "Multiscale Computations of Parameters of Power Transformer Windings at High Frequencies. Part I: Small-Scale Level," *IEEE Transactions on Magnetics*, vol. 43, no. 11, pp. 3991-3998, 2007.
- [13] J.-R. Sibue, J.-P. Ferrieux, G. Meunier, and R. Periot, "Modeling of Losses and Current Density Distribution in Conductors of a Large Air-Gap Transformer Using Homogenization and 3-D FEM," *IEEE Transactions* on Magnetics, vol. 48, no. 2, pp. 763-766, 2012.
- [14] Y. Otomo, H. Igarashi, H. Sano, and T. Yamada, "Analysis of Litz Wire Losses Using Homogenization-Based FEM," *IEEE Transactions on Magnetics*, vol. 57, no. 8, pp. 1-9, 2021.

- [15] R. V. Sabariego, P. Dular, and J. Gyselinck, "Time-Domain Homogenization of Windings in 3-D Finite Element Models," *IEEE Transactions on Magnetics*, vol. 44, no. 6, pp. 1302-1305, 2008.
- [16] J. Gyselinck, R. V. Sabariego, and P. Dular, "Time-Domain Homogenization of Windings in 2-D Finite Element Models," *IEEE Transactions on Magnetics*, vol. 43, no. 4, pp. 1297-1300, 2007.
- [17] A. Robkopf, C. Joffe, and E. Bar, "Calculation of ohmic losses in litz wires by coupling analytical and numerical methods," in 2014 4th International Electric Drives Production Conference (EDPC), Nuremberg, Germany, 2014 2014: IEEE, pp. 1-6.
- [18] H. Igarashi, "Semi-Analytical Approach for Finite-Element Analysis of Multi-Turn Coil Considering Skin and Proximity Effects," *IEEE Transactions on Magnetics*, vol. 53, no. 1, pp. 1-7, 2017.
- [19] D. Lin, C. Lu, N. Chen, and P. Zhou, "An Efficient Method for Litz-Wire AC Loss Computation in Transient Finite Element Analysis," *IEEE Transactions on Magnetics*, vol. 58, no. 5, pp. 1-10, 2022.
- [20] C. R. Sullivan, "Optimal choice for number of strands in a litz-wire transformer winding," *IEEE Transactions on Power Electronics*, vol. 14, no. 2, pp. 283-291, 1999.
- [21] J. Ferreira, "Analytical computation of ac resistance of round and rectangular litz wire windings," in *IEE Proceedings B (Electric Power Applications)*, 1992, vol. 139, no. 1: IET, pp. 21-25.
- [22] H. Rossmanith, M. Doebroenti, M. Albach, and D. Exner, "Measurement and Characterization of High Frequency Losses in Nonideal Litz Wires," *IEEE Transactions on Power Electronics*, vol. 26, no. 11, pp. 3386-3394, 2011.
- [23] J. T. Shi, R. P. Deodhar, C. Umemura, and A. Pride, "Comprehensive Study of Variable Flux Memory Machines with Symmetrical Series Hybrid Permanent Magnets in Rotor Pole," (in English), 2020 International Conference on Electrical Machines (Icem), Vol 1, pp. 619-625, 2020.
- [24] A. Krings and C. Monissen, "Review and Trends in Electric Traction Motors for Battery Electric and Hybrid Vehicles," 2020 International Conference on Electrical Machines (ICEM), Gothenburg, Sweden, 2020, pp. 1807-1813.